Electron Emission and Plasma Formation During Laser Beam Welding

Optical radiation emitted by the plasma is useful for monitoring purposes, and plasma generation can be monitored using microphones

BY R. D. DIXON AND G. K. LEWIS

ABSTRACT. A 400 watt average power Nd-YAG laser (1.06 micrometer wavelength) was used to study the effects of plasma generation on welding. Laser spot welds on aluminum and stainless steel were monitored optically, acoustically and electrically.

Results show that the laser is optically coupled to the workpiece, significant current is emitted by the workpiece, current can be detected from the plasma, optical radiation emitted by the plasma is useful for monitoring purposes, and plasma generation can be monitored using microphones. The plasmas propagate as laser supported combustion waves and are expected to contribute significantly to heat input during welding.

Introduction

In previous papers (Refs. 1, 2) and presentations (Refs. 3, 4), a model for laser beam welding requiring the creation of a plasma has been discussed. The basis for the model was extracted from the literature (Ref. 5-10) and extended to laser beam welding. Essentially, the model shows that the plasma is responsible for the increase in heat input, above that from absorption of laser radiation alone. This phenomenon is known as enhanced coupling.

The plasma generated is described as a laser supported combustion (LSC) wave whose heat output, when combined with that of the laser, can approach 50% of the total power available from the laser (Ref. 5). For example, if the linear absorption of 1.06 μm (4.2×10^{-5} in.) laser radiation by an aluminum (Al) sample is approximately 10%, then with maximum enhanced coupling the absorption increases to 50%. Here the plasma appears to make a contribution four times that of the laser. Because the plasma can have such a significant effect upon the heat input, it is essential to know more about it.

The laser-material-interactions (LMI) described in the literature are for short pulse length (<100 μs, *i.e.*, <0.0001 s) laser systems. Welding laser units typically operate with pulse lengths much greater than 100 μs. Thus, our work extended the interpretation of LMI to those long pulse lengths. We have shown that, during one laser beam welding pulse, multiple plasmas are generated, each preceded by an acoustic pulse. The number of plasmas generated is then proportional to observable weld effects. This has been verified by high speed movies, plasma radiation detection using a photomultiplier tube (PMT), and acoustic monitoring. (A more complete description is available in the literature, *i.e.*, Refs. 1, 2.)

One phenomenon associated with laser beam welding and the plasma that has received little attention is the current emitted to form and maintain the plasma. Data on electron current behavior as a function of time yields information about the plasma formation, lifetime and decay. This, coupled with the fact that early work at our lab gave no attention to grounding the weldment, prompted this study. In the next section thermoelectron emission is shown to yield a large number of electrons, and for the proper geometry a large field could be created outside of an ungrounded (floating) part. Subsequent sections deal with the plasma, experimental work, results and discussion.

Paper presented at the 65th Annual AWS Convention in Dallas, Texas, during April 8-13, 1984, under sponsorship of the DOE Interagency Group.

R. D. DIXON and G. K. LEWIS are with the Materials Science and Technology Division, Los Alamos National Laboratory, Los Alamos, New Mexico.

Sources of Current

Laser breakdown is defined as ionization of a cold gas and the initial appearance of a plasma, whether in air or with a surface present; it requires a significant number of electrons for initiation. The electrons originate by several mechanisms within the material as well as in the environment (gas) above the material surface. Electrons are generated in the gas by multiphoton and electron cascade mechanisms, neither of which is likely to provide the electron densities needed for breakdown with our system. Of the two, however, the multiphoton process has the greater probability for electron creation at the power densities and energies of the welding laser.

Electrons are generated from the material by thermoelectron and photoelectron processes. Here again the photoelectron effect is a multiphoton process which will contribute some electrons. The magnitude cannot be easily determined because of the nonlinear nature of the process. The thermoelectric current density can be estimated from classical physics using the Richardson-Dushman equation:

$$J = AT^2 e^{-\phi/KT} \qquad (1)$$

where J = thermoelectric current density, A = const = 120 amperes cm^{-2} deg^{-2}, T = absolute temperature, k = Boltzmann's constant,* and ϕ = work function of the material.

Using equation (1) and the constants as

**K as Boltzmann's constant to be distinguished from K for Kelvin which is a measure of temperature (1K = −273°C = −459°F).*

RESEARCH/DEVELOPMENT/RESEARCH/DEVELOPMENT/RESEARCH/DEVELOPMENT/RESEARCH/DEVELOPMENT/RESEARCH/DEVELOPMENT

Table 1—Calculated Thermoelectric Current Densities at the Melting Points

	Aluminum	Stainless steel
Work function, ev	3.74	4.5
Current density, A/cm^2	1.8×10^{-11}	2.1×10^{-7}
No. electrons/cm^2	1.1×10^{8}	1.3×10^{12}

defined in Table 1 yields the current densities shown in the table. From Table 1, it is seen that at their melting points a significant number of electrons are emitted by both aluminum and stainless steel. Assuming boiling points of 2700 and 3000 K (1 K = −273°C = −459°F) for aluminum and stainless steel, respectively, yields electron densities on the order of 10^{20} electrons per cm^2. Also from Table 1, one notes that the difference in the work functions of these materials is only 0.75 eV. Using equation (1), this results in a 10^4 difference in electron density. Thus small variations in the work function can greatly affect the thermoelectric current.

In addition to contributing to the breakdown process, the emitted current could also create a charge on any weldment which is not grounded. The effect is, of course, dependent upon the part size and is greatest for small parts or ones with sharp points. The effect will not, in general, produce a large enough charge to cause a safety problem but will influence the emission current by increasing the effective work function.

Using the example from Table 1 with an emission area of 0.05 mm (0.0032 in.^{2}), a 0.2 mm (0.0008 in.) diameter aluminum sphere will acquire a potential of only 0.006 V during a 7.8 ms laser weld. However, electron emission in excess of 10^{11} electrons was measured during the experiments. This is 3 orders of magnitude greater than the calculation, and thus charge build-up could be a problem. Using the above example, with 10^{11} electrons per second, a very high potential (several hundred volts) could be produced and would have a major influence on electron emission.

After the electrons are emitted, they will gain energy through free-free and free-bound interactions supported by the incident and reflected laser radiation. This continues until the laser radiation is totally absorbed at which time the plasma is said to be fully ignited. For our applied power levels, the plasma propagates as a LSC wave preceded by a pressure wave with velocity less than or equal to the sound velocity (Refs. 1, 2). A LSC wave is defined as a plasma propagating with a subsonic velocity. This phenomenon is also discussed in the literature (Refs. 5, 6).

The LSC wave propagates back through the laser beam, dissipating energy through blackbody radiation and lateral expansion. The plasma also decays because of the decreased input power density as a result of the beam focusing divergence. At some time during the plasma decay, the laser radiation again impinges on the heated target, penetrating an already reasonably high density plasma; and another LSC wave is generated. This process is repeated throughout the laser pulse. Thus, numerous LSC waves are generated, each heating the surface with radiation which is essentially blackbody in nature. The target surface is also heated by the laser radiation during those times, when it is not totally absorbed by the LSC wave.

It was expected that this modulated heat input (proportional to the number of plasmas generated) could be detected as thermoelectric current from the part and from current which drifts from the LSC wave as it expands.

Experimental

An experiment was designed to test the theory that the current emission from the target and plasma could be detected and would indicate the existence of the plasmas. The current signals were compared to the signal obtained from a photomultiplier tube (PMT) having an S-20* response. The PMT was fiber optically coupled to the laser-target interaction (LTI) region and detected the onset of visible radiation emission.

Two microphones were positioned opposite each other and in line with the target spot to detect the precursor pressure wave. They were displaced unequally from the LTI region so that the pressure wave velocity could be measured.

The LTI region was contained in an electrically shielded box so that high gain current measurements could be made. The current was monitored using commercial amplifiers capable of gains from 10^4 through 10^{11} volts per ampere. Current from the plasma was detected using a 1 in. (25.4 mm) long cylindrical collector placed 6.4 mm (0.25 in.) away from the sample surface and coaxial with the laser beam.

The collector was unbiased so that only current drifting from the plasma was detected. Difficulty in measuring the plasma drift current resulted from the location of the plasma current detector. Since the plasma current collector was shielded from the target to eliminate any coupling, the shielding provided a surface for drift current from near the target to collect and diminished the current detected. Sufficient current was available, however, to be detected.

The targets used were 22 mm (0.85 in.) in diameter by 1.6 mm (0.62 in.) thick and mounted on a rotating base. This mounting, by rotation, allowed a number of pulses to impinge on fresh surfaces and located the spots at a constant radius. After the maximum number of spots were placed on each specimen, the spot diameters were measured and the target was then machined to the center of each spot for melt depth (penetration) measurements. All laser beam welds were done in one atmosphere of air without cover or shielding gas.

The materials used were commercial heats of aluminum alloys 6061, 1100, and 5052 as well as Type 304 stainless steel (SS). The laser impingement spot was cleaned with alcohol prior to each pulse, and only one pulse was incident on each spot.

The laser used was a pulsed Nd-YAG (1.06 micron wavelength, *i.e.*, 1.06 μm or 4.2×10^{-5} in.) system capable of a maximum average power of 400 watts (W) and a maximum energy of 50 joules per pulse. The pulse length was varied from 3.8 to 7.8 ms with a constant pulse rate of 10 pulses/s. Single pulse welds were made at sharp visual focus without an aperture in the beam path. The power was measured for each condition using a Coherent model 213 power meter.

The laser pulse shape was displayed and monitored on a scope and was approximately the same for each pulse length used. The pulse shape, length and repetition rate were monitored on an oscilloscope using a detector on the back of the laser cavity coupled with a 0.01% transmitting rear cavity mirror. This signal was also recorded on the digital oscilloscope as the "Laser Signal." The laser beam diameter at sharp focus was determined from burn patterns, for each power and pulse length used. The pulse length was measured from the scope traces and was taken as the difference between zero voltage times at the start and end of the pulse.

All data were recorded on digital storage oscilloscopes at a rate of 2 microseconds (μs) per data point. A four channel scope was used to monitor the rear cavity detector (laser signal), PMT and two microphone outputs. A two channel scope was used to monitor the target emission current and the plasma drift current. The two channel scope was

"S-20" is the standard term used to describe quantum optical detectors with a given spectral sensitivity. All S-20 detectors have the same spectral sensitivity which is an industry standard.

slaved to the four channel scope for triggering.

The trigger source was a logic circuit that produced a pulse when both the laser shutter was open and the next laser pulse occurred. The trigger pulse also triggered a delay pulse generator that output a pulse into one channel of each scope delayed by the laser pulse length minus 0.4 millisecond (ms). This was done to allow accurate correlations between the data from both scopes.

Figure 1 is a schematic diagram of the experimental setup, and Table 2 shows the experimental conditions used.

Results and Discussion

Pressure Wave Velocity

The pressure wave velocity was measured for all data taken. The velocities were all found to be independent of material, pulse length and power and equalled the sound velocity. This indicates that the plasma waves generated were indeed LSC waves. The LSC waves are those which have been determined to contribute the maximum radiation to the target.

Peak Power vs. Average Power

In all plots to follow, the dependent variable is plotted against intensity (I) (pulse power density in watts (W) per cm^2). Intensity was determined from:

$$I = \frac{\overline{P}}{A} = \frac{1}{TA}\int Pdt \simeq \frac{\Sigma P\Delta T}{TA} = \frac{NP\Delta T}{TA} \qquad (2)$$

where $\overline{P}$ = average power, T = integration period, A = beam area at $\overline{P}$, P = pulse power, N = pulse rate and ΔT = pulse length.

The average power and beam area were measured for each experimental condition. The beam area was determined by measuring the hole burned in black photographic paper.

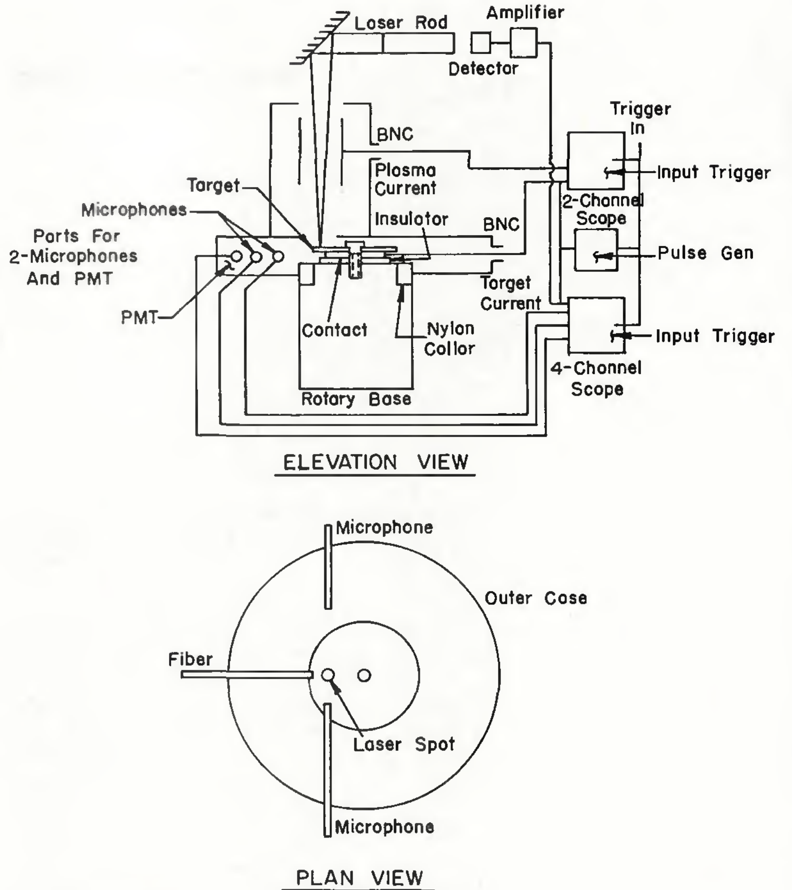

Fig. 1—Diagram of experimental setup

Laser Isolation

During this and previous studies, it was observed that the laser signal (signal from the detector at the rear of the cavity) varied in structure depending upon the power and material being irradiated. This structure is shown in Fig. 2 as the small amplitude signals superimposed on the continuous background. The structure is random in time and each occurrence has a finite duration. The initiation times of the structure qualitatively correlate with plasma initiation times and with periods of low plasma radiation emission as seen in PMT spectra shown in Fig. 3.

The source of this signal was not the laser flash lamp, and thus it originated outside the laser cavity. The only possibility was the laser-target region. This structure was, therefore, the result of reflection of the laser radiation from the target or plasma back through the laser rod. Based on this correlation, the time at which the structure initially diminishes was used as a measure of plasma initiation and is discussed elsewhere in this paper.

This phenomenon could potentially be used to monitor plasma generation during the weld. For our work the number of plasmas detected using the PMT did not correlate with the number of plasmas detected by counting structure regions in the laser signal. This is due to the time and amplitude resolution of the laser signal.

The effect of this reflection on overall laser performance is not known at this time. Since data were taken at 2 μs per point during the experiments and since the laser rod emission should show structure in the nanosecond and subnanosecond time frames, the absolute behavior of the laser during these periods is

Table 2—Experimental Conditions

Av. power, W	Pulse length, ms	Material
50	7.8	6061 aluminum
100		1100 aluminum
150		5052 aluminum
200		Type 304 stainless steel
250		
275		
300		
325		
100	5.6	1100 aluminum
250		5052 aluminum
		Type 304 stainless steel
100	3.8	6061 aluminum
		1100 aluminum
		5052 aluminum
		Type 304 stainless steel

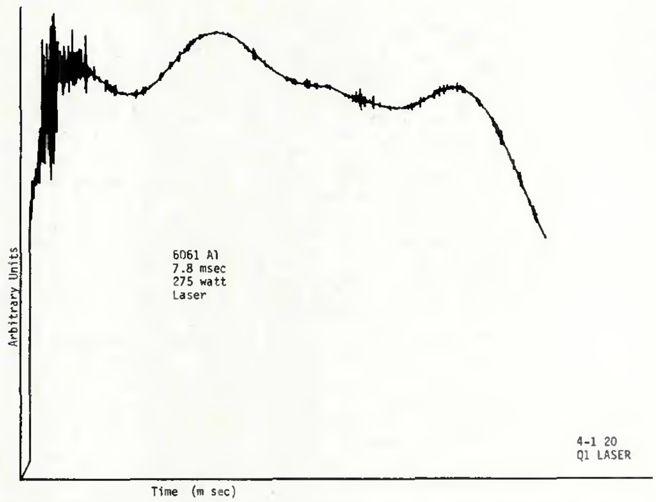

Fig. 2 — Laser signal from 275 W average power on 6061 aluminum alloy. Shows structure resulting from laser coupled to the target. Pulse length is determined from zero voltage crossings

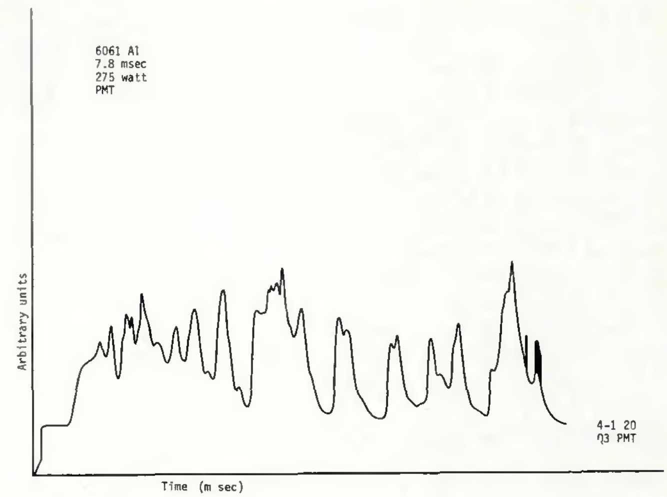

Fig. 3 — PMT signal from 275 W average power on 6061 aluminum alloy. The first inflection point determines the initiation time and each peak signals a plasma initiated

unknown. It is most likely that these reflections will both decrease the beam quality and total energy.

The phenomenon may be important for reliable control of laser welding machines and thus be essential to laser beam weld quality control.

Initiation Time

Plasma initiation times were determined from the PMT, target current emission, plasma current emission and laser signals. The initiation times from the PMT, target current and plasma current were determined as the first inflection points of the signals. The initiation time from the laser signal was taken as the time at which the initial structure (as previously discussed) disappeared.

Plots of data for the four different materials used are shown in Figs. 4–7. For these and subsequent graphs, the data taken at different pulse lengths are indicated in the upper margin of each plot with the balance of the data from 7.8 ms pulses. With the exception of the low I target current initiation data from 6061 aluminum, the trends are the same. The initiation times are large for low I and monotonically decrease as I increases.

For aluminum at any I, the initiation time is less when determined from the PMT signal than from the other signals. Also, all initiation times approach a different constant value for large I with that from the PMT being the smallest. For the Type 304 stainless steel, the low I initiation times are less than the high I initiation times on Al. It is also noted that, within experimental error, the initiation times determined from the target current are less than these determined from the PMT although there is very little difference.

The curves drawn in Figs. 4–7 are not numerically fit or theoretical. They were fitted by inspection of the data and serve only to draw attention to the data trends. It can be noted, however, that the initiation times determined from the PMT are the most consistent, while those from the plasma are the least consistent. The large scatter seen in several of these illustrations is a result of welds at or greater than 100% penetration and the shielding geometry used in the current detection setup.

The aluminum alloys both have faster initiation times at high I than the commercially pure metal but beyond that there is no consistent behavior. It is also worth noting that the initiation times determined by the structure on the laser signal are monotonically decreasing as expected. This indicates that the laser signal may be a monitor of more than just the laser

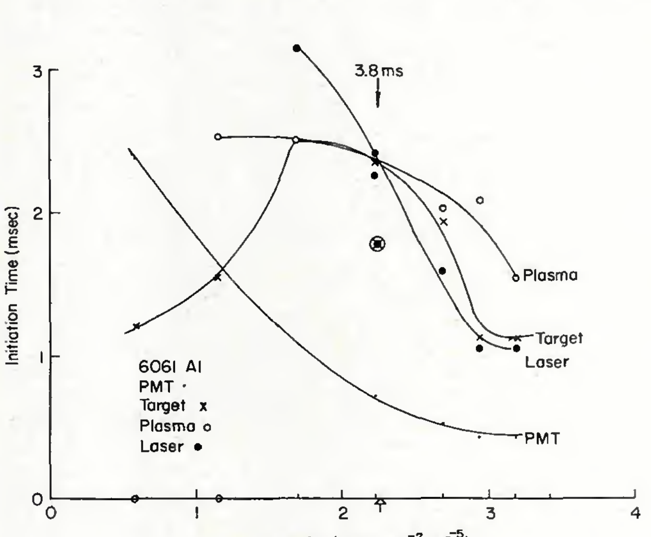

Fig. 4 — Initiation times from PMT, target current, plasma current and laser signals vs. I for 6061 aluminum alloy

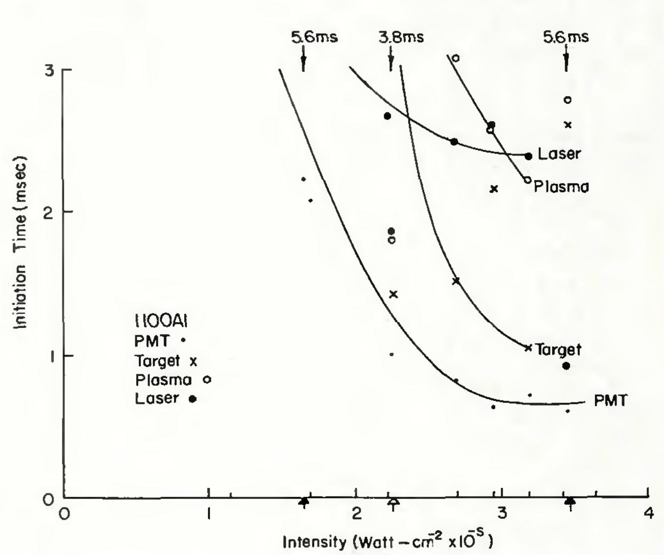

Fig. 5 — Initiation times from PMT, target current, plasma current and laser signals vs. I for 1100 aluminum alloy

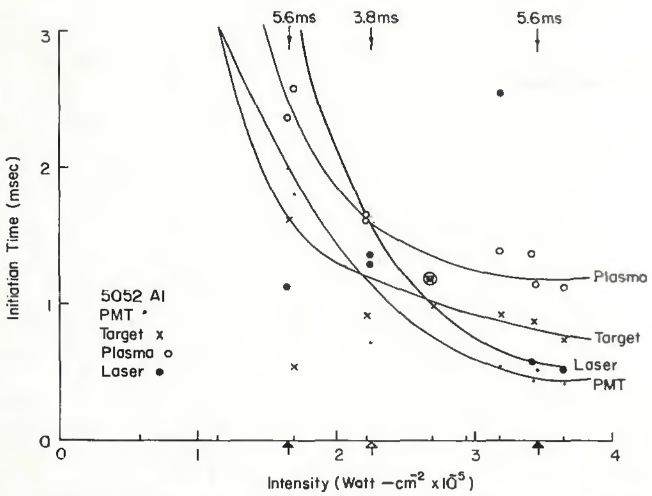

Fig. 6—Initiation times from PMT, target current, plasma current and laser signals vs. I for 5052 aluminum alloy

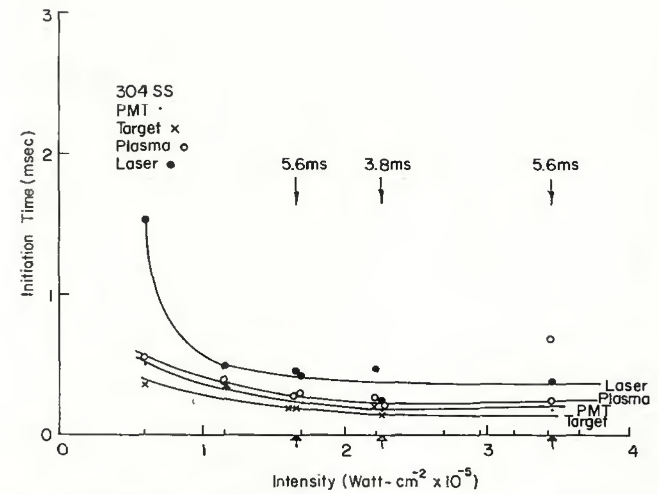

Fig. 7—Initiation times from PMT, target current, plasma current and laser signals vs. I for Type 304 stainless steel

pulse shape.

Number of Plasmas

The number of plasmas per second (s) vs. I for all materials are shown in Figs. 8-11. The number of plasmas/s was determined in each case by counting the total number of plasmas in the signal and dividing by the pulse length minus the initiation time for the PMT, and by the current duration minus the initiation time for the target electron emission and the plasma electron emission. Here again, the solid curves were fitted by inspection of the data.

Figures 8-11 can be interpreted when reviewed along with the penetration and spot size data vs. I, shown in Figs. 12 and 13, respectively. For the aluminum alloys, at intensities between 2.1 and 2.5 $\times$ 10^5 W cm^{-2}, the penetration goes from incomplete to complete. The transition from small to approximately constant larger spot size occurs across the I range of 1.75 to 3.1 $\times$ 10^5 W cm^{-2}. Thus, up to complete penetration the number of plasmas per unit time increases, for all materials studied.

For intensities in excess of those needed for 100% penetration, the cavity wall provides sufficient electrons and vapors to form plasmas, heat the material, and expand the heated regions. The number of plasmas generated beyond complete penetration is a complicated function of the cavity behavior as indicated by the data. At I's equal to or greater than a maximum spot size, with complete penetration the number of plasmas per unit time appears to decrease. This could be a result of the decreased heat input per unit area and thus material available for plasma generation. Thus the scatter seen in these illustrations is a result of the welds being 100% or greater in depth.

Emission Current

Figures 14-16 are typical examples of the target emission current, plasma drift current, and integrated target emission current signals. Figures 14 and 15 show typical examples of the initiation time and current fluctuations (interpreted as plasma initiations) obtained during the study. To analyze the current behavior, the average current, defined in equation (4), was scaled to the maximum gain and divided by the spot size (equation 3) then plotted against I:

$$J = I_0 \cdot 10^9/[(\text{gain at I})(A)] \qquad (3)$$

where J = average current density, 10^9 = maximum gain used in this study, and A = spot size (mm^2).

The data are average current densities

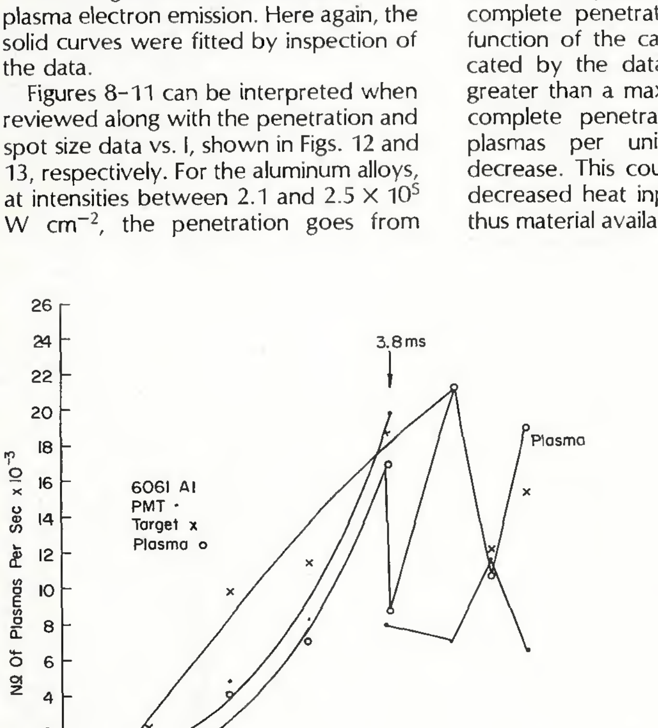

Fig. 8—Number of plasmas/s from PMT, target current and plasma current signals vs. I for 6061 aluminum alloy

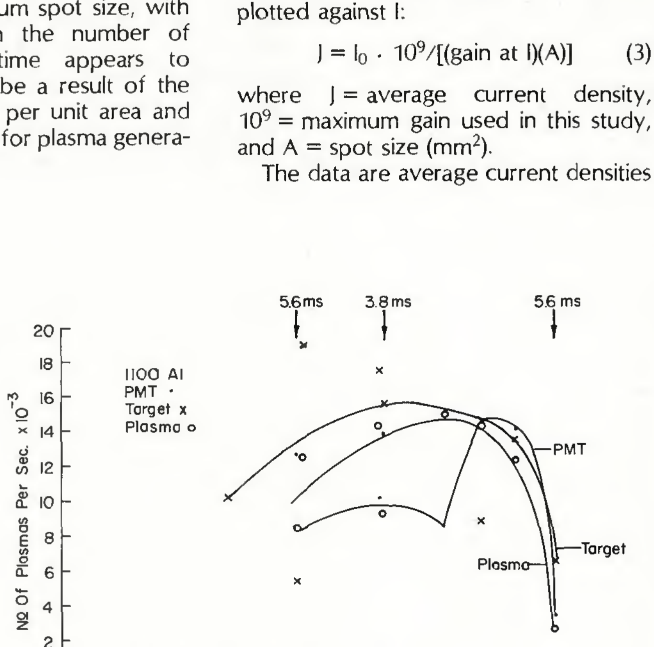

Fig. 9—Number of plasmas/s from PMT, target current and plasma current signals vs. I for 1100 aluminum alloy

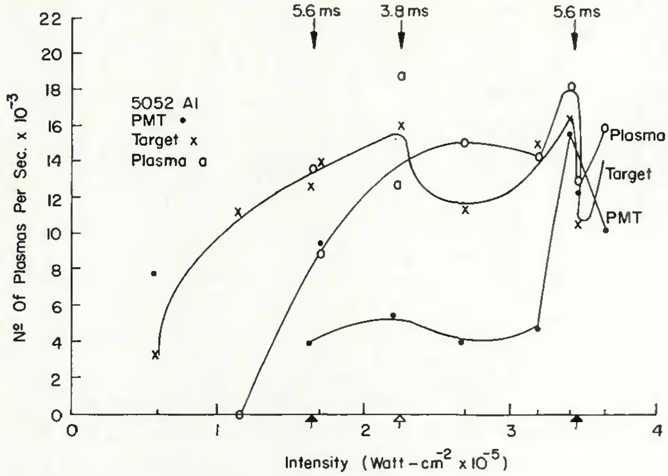

Fig. 10—Number of plasmas/s from PMT, target current and plasma current signals vs. I for 5052 aluminum alloy

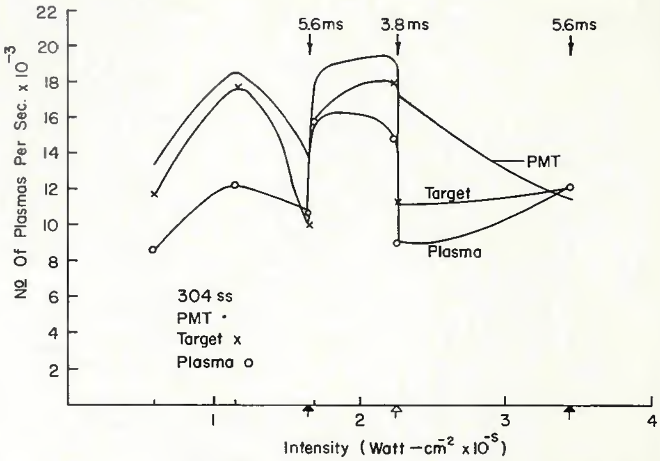

Fig. 11—Number of plasmas/s from PMT, target current and plasma current signals vs. I for Type 304 stainless steel

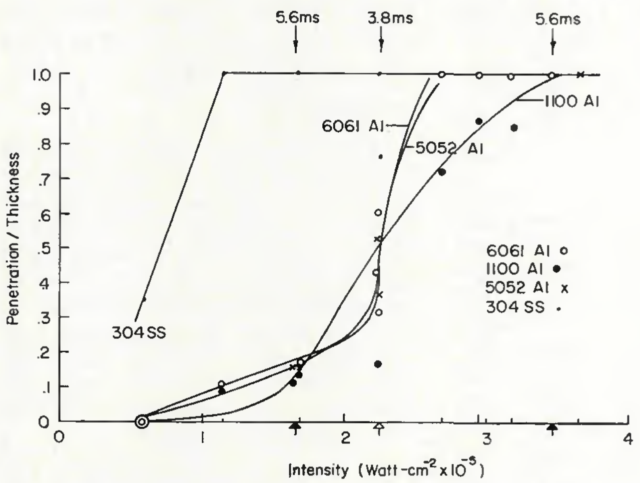

Fig. 12—Penetration divided by target thickness vs. I for all materials studied

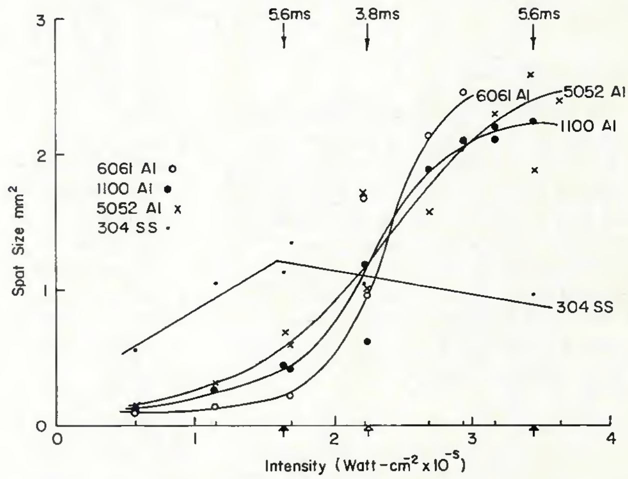

Fig. 13—Spot size vs. I for all materials studied

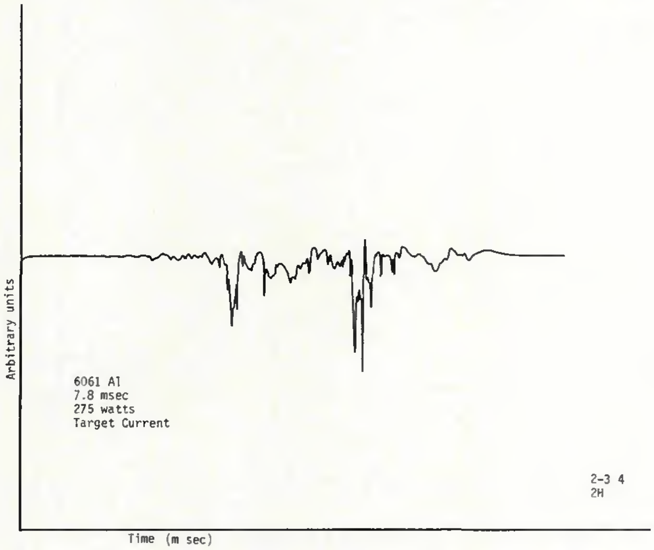

Fig. 14—Example of target current signal. Data from 275 W on 6061 aluminum alloy using 7.8 ms pulse

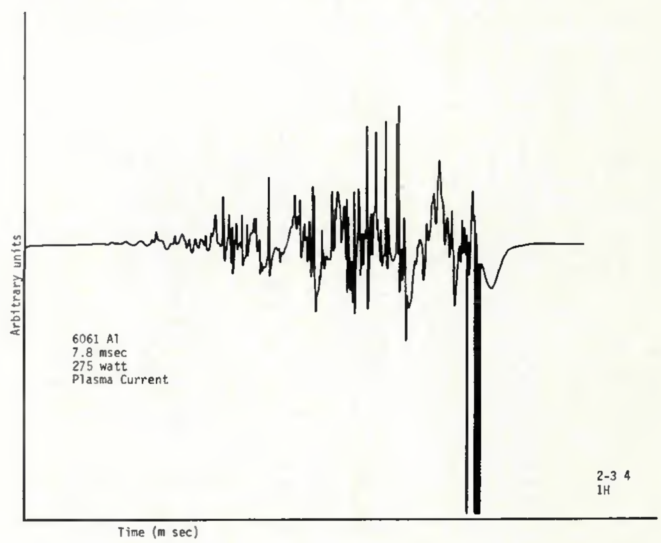

Fig. 15—Example of plasma current signal. Data from 275 W on 6061 aluminum alloy using 7.8 ms pulse

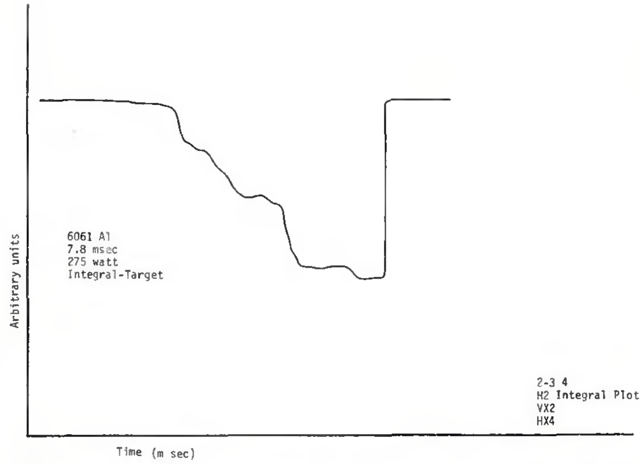

Fig. 16 — Example of integrated target current signal. Data from 275 W on 6061 aluminum alloy using 7.8 ms pulse

and are shown in Figs. 17–20 where the data were again fitted by inspection. Figure 16 shows the integral of Fig. 14, with:

$$I_0 = \frac{1}{T} I_0 \, dt \quad (4)$$

where I_0 = average current, T = period for integration, I_0 = instantaneous current, and dt = time interval.

The data are normalized for direct comparison by scaling to the maximum gain. One feature noted is that the target current is greater than the plasma drift current. This is to be expected from the collection geometry.

Electron emission from 1100 aluminum has a threshold intensity of 1.5×10^5 W cm^{-2}. 5052 and 6061 aluminum have thresholds at about 2.25×10^5 W cm^{-2} and behave similarly up to 3.25×10^5 W cm^{-2}. The maximum current measured ranged from approximately 3×10^{-8} amperes for 1100 aluminum to 3×10^{-6} amperes for 5052 aluminum, with 6061 aluminum and Type 304 stainless steel in between. This correlates to a maximum electron emission of from approximately 1×10^9 to 1×10^{11} electrons per pulse for these materials, respectively.

With this number of electrons from the target, there are sufficient electrons to achieve the electron density required to totally absorb the laser radiation. In fact, it may be possible for the electron density to reach the critical density for 1.06 μm (4.2×10^{-5} in.) radiation at which time the laser radiation is completely reflected. This density for the 1.06 μm radiation is approximately 3×10^{20} electrons · cm^{-2}.

For 5052 and 6061 aluminum, the target electron emission increased uniformly up to the point of maximum spot size and 100% joint penetration. Here again, however, the dynamics associated with 100% joint penetration can be expected to contribute to the observed behavior. Also, for these two alloys the electron emission threshold was about the same as the penetration threshold. For 1100 aluminum, the electron emission threshold occurred well before the penetration threshold; in fact, the emission spectrum peaked at about the penetration threshold.

For the Type 304 stainless steel, the electron emission threshold is approximately the same as the penetration threshold with electron emission continuing well beyond 100% penetration and maximum spot size. This behavior is probably the result of the higher melting point and heat capacity of the steel.

In all cases, the electron emission current can be measured and is a relatively large quantity.

Conclusion

Weld morphology vs. intensity shows the expected threshold behavior (*i.e.*, low penetration up to a threshold after which penetration significantly increases) which is different for aluminum alloys from that for Type 304 stainless steel. Several data points were taken at power levels that produced penetrations of 100%.

The laser obviously couples to the target (*i.e.*, extension of the cavity to the workpiece), but the effect of this on weld morphology or other variables is unknown. The structure on this signal can, however, be used as a means of monitoring plasma initiation.

Plasma initiation and the number of plasmas generated can be monitored by optical radiation, laser cavity response, target current or plasma drift current. The data obtained by monitoring the optical radiation from the plasma (PMT signal) are always monitonically decreasing with intensity. The data from the target current, plasma current and the laser signal have no trends.

There is considerable current emitted

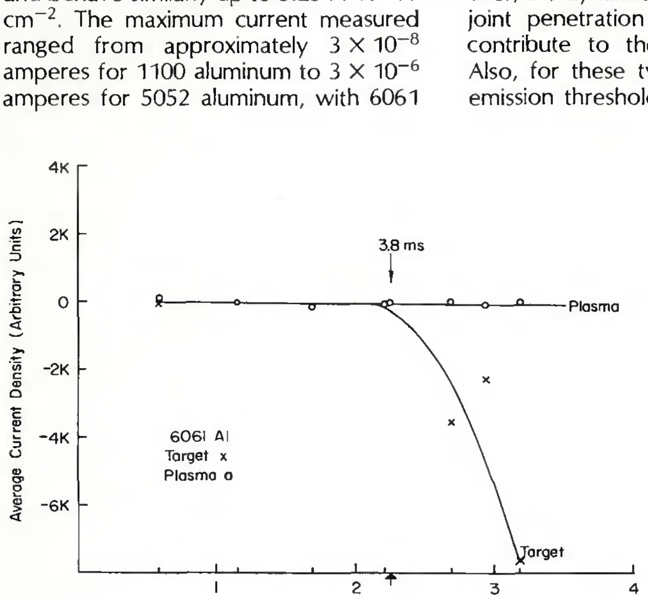

Fig. 17 — Average current density from the target and the plasma vs. I for 6061 aluminum alloy

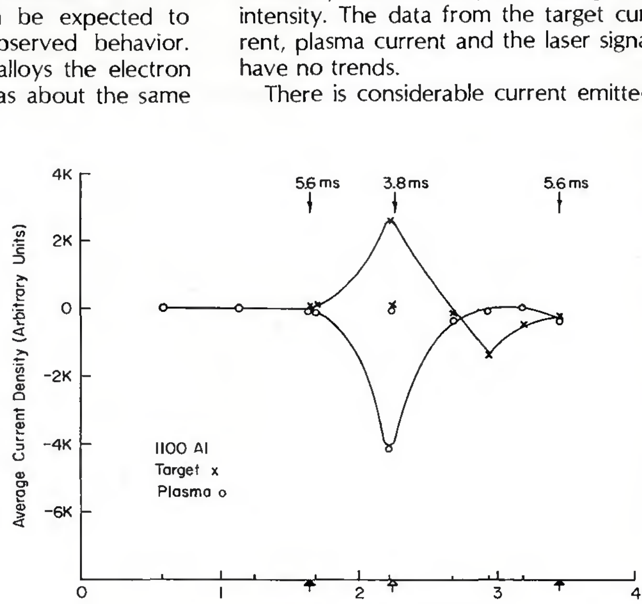

Fig. 18 — Average current density from the target and the plasma vs. I for 1100 aluminum alloy

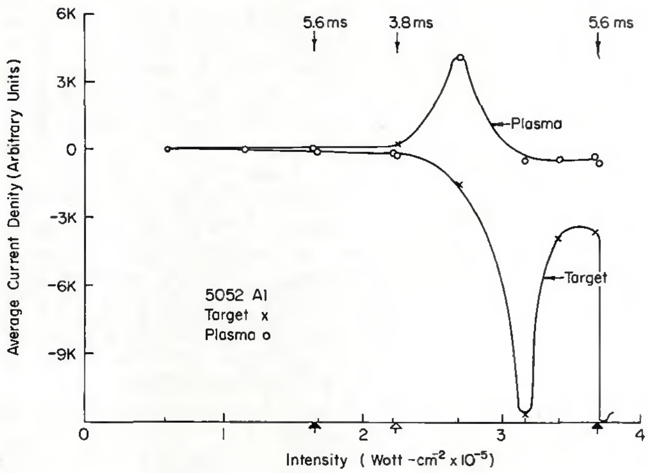

Fig. 19—Average current density from the target and the plasma vs. I for 5052 aluminum alloy

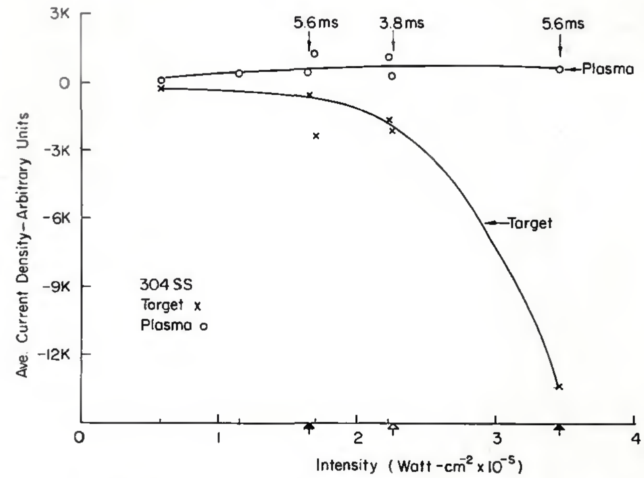

Fig. 20—Average current density from the target and the plasma vs. I for Type 304 stainless steel

from all materials studied. The current is measurable and should be considered when setting up laser welds. Without grounding a workpiece, a charge can build up on it. The charge is not a safety hazard; however, it greatly influences the plasma through decreased electron emission resulting from changing the effective work function. This, in turn, reduces the number of plasmas generated and consequently the heat input. The electron densities observed support the concept of 100% laser radiation absorption and could approach the critical density.

Material properties such as heat capacity, thermal conductivity, thermal diffusivity, work function and surface oxidation influence the behavior of the emission current after 100% penetration and maximum spot size are achieved.

Current can be collected from the plasma but there is no trend to the data. This signal is also subject to the geometry of the collector.

All plasmas generated at these power levels are described as LSC waves and multiple plasmas are generated during each laser beam weld.

References

1. Dixon, R. D., and Lewis, G. K. 1985. Plasma monitoring of laser welds. *Welding Journal* 64(2): 000-s to 000-s.

2. Dixon, R. D., and Lewis, G. K. 1983. The influence of a plasma during laser welding. *Proceedings of the 1983 ICALEO.*

3. Lewis, G. K., Rollett, A., Schwalbe, L., Flick, F., and Ward, W. 1983. Acoustic emission and plasma light source monitoring of laser welds. American Welding Society Annual Meeting, April 1983.

4. Lewis, G. K., and Dixon, R. D. 1984. Observed effects of plasma formation and enhanced coupling during laser welding. WESTEC, March 1984.

5. Pirri, A. N., Kemp, N. H., Root, R. G., and Wu, R. K. S. 1977 (Jan.). *Theoretical laser effects studies.* Final report, PSI-TR-89, Physical Sciences, Inc.

6. Boni, A. A., Su, F. V., Thomas, P. D., and Musal, H. M. 1977 (April). *Theoretical Study of Laser Target Interaction.* Final Report, SAI-77-567 LJ, Science Applications, Inc.

7. Pirri, A. N., Root, R. G., and Wu, P. K. S. 1978. Plasma energy transfer to metal surfaces irradiated by pulsed lasers. *AIAA Journal* 15(12):1296-1304.

8. Raizer, Q. P. 1965. (Nov.). Heating of a gas by a powerful light pulse. *Soviet Physics JEPT* 21(5):1009-1017.

9. Jackson, J. P., and Nielson, P. E. 1974. Ignition transients and two-dimensional effects in the propagation of laser-supported-absorption waves. *Laser Digest,* report AFWL-TR-74-100:212-226.

10. Boni, A. A., and Su, F. Y. 1974 (Feb.). Propagation of laser supported deflagration waves. *The Physics of Fluids* 17(2):304-342.

WRC Bulletin 300
December 1984

Under the direction of the Steering Committee on Piping Systems of the Pressure Vessel Research Committee of the Welding Research Council, the Technical Committee on Piping Systems developed a document on criteria establishment describing their objectives and accomplishments, and three technical position documents that have an effect on the design of piping systems, entitled: 1) Technical Position on Criteria Establishment; 2) Technical Position on Damping Values for Piping Interim Summary; 3) Technical Position on Response Spectra Broadening; and 4) Technical Position on Industry Practice.

The technical Position Documents have been submitted to the ASME Boiler and Pressure Vessel Code Committee and the U. S. Nuclear Regulatory Commission for their use.

The price of WRC Bulletin 300 is $14.00 per copy, plus $5.00 for postage and handling. Orders should be sent with payment to the Welding Research Council, Rm. 1301, 345 E. 47 St., New York, NY 10017.